

ACM Report, January 2019

LCRD Sun Scintillometer

Janet P. Wu and Sabino Piazzolla

Table of Contents

Contents

Abstract	3
1 Basic System Description.....	4
1.1 Hardware and Alignment	4
2 Software.....	5
2.1 Start Up Operation	5
2.2 Task Scheduler Settings	5
2.1.1 Open Task Scheduler.....	5
2.1.2 View task properties	6
2.1.3 How to update program daily start time	7
2.1.4 How to update program executable file location.....	7
2.2 Manual Software Startup and Exit (If Needed)	8
2.3 Terminal Window Display	9
3 Data File.....	10
4 Theory.....	11
5 Data Analysis.....	12
6 Data Structure.....	14
7 Data Description	15
8 Filtering of the data	17
8.1 Saturation Values.....	17
8.2 Thesholding Lower Values.....	18
8.3 Monthly Statistics	21
9 References	24

Abstract

In 2017 a new Sun Scintillometer was installed on the roof to the OCTL to monitor daytime turbulence and to provide measurement of the atmospheric coherence length (also known as Fried parameter or r_0) during daytime. This instrument will provide initial real time measurement of daytime optical turbulence for the LCRD program.

In this report, we first describe the software and the hardware of the Sun Scintillometer. Next, we introduce Sun Scintillometer theory and the validation of the measurements compared with measurements from another instrument, namely a Solar DIMM. Finally, we discuss the data filtering and statistics from the OCTL's Sun Scintillometer.

1 Basic System Description

The instrument measures light intensity fluctuations (scintillation) from Sun's observations. These measurements are used to determine daytime astronomical seeing and/or atmospheric coherence length (r_o) along the line of sight between the ground sensor and the Sun. A brief description of the system is provided in this section. Details of the methodology and instrument design can be found in references [1] and [2].

1.1 Hardware and Alignment

The hardware consists of a small sensor (i.e. large area APD sensible in the visible) connected to an external custom electronics board as shown in Figure 1. The sensor is encased by a clear hemispherical window and has a relatively wide field of view. It is mounted in a fixed position pointing in the direction of the Sun at peak elevation angle. The sensor alignment is usually performed around local noon time and ideally adjusted four times a year to account for the seasonal changes in maximum Sun elevation angle. The alignment process is relatively simple in which the sensor head is pointed directly at the Sun and rotated in azimuth and elevation until the size of its shadow on the ground is minimized. The sensor provides measurements of

The external electronics board processes the input sensor signal and the resulting voltages are output through a RS232 serial USB interface to connect with a computer. The computer USB connection also powers the board and sensor.

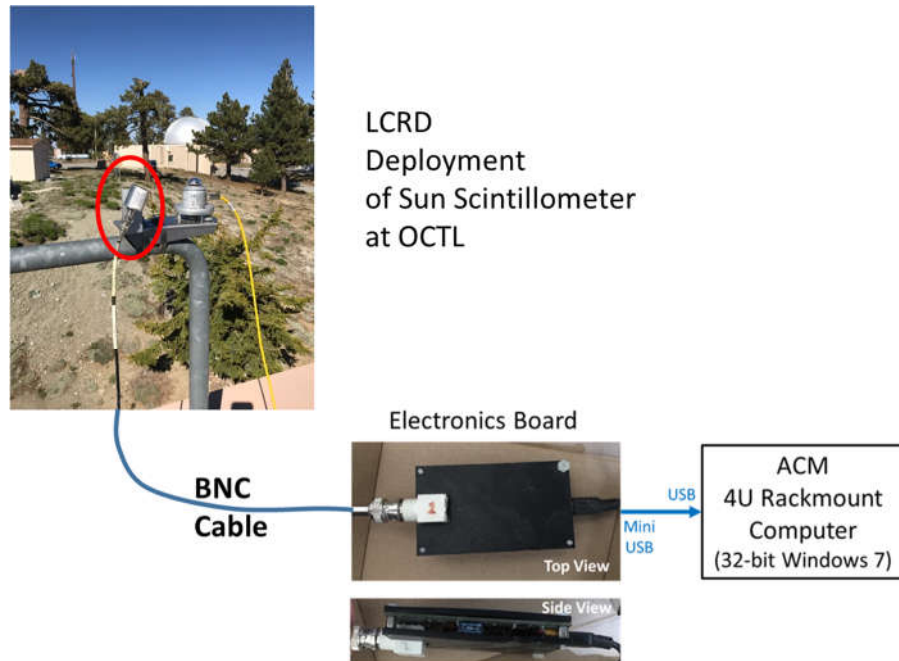


Figure 1: Sun scintillometer system hardware components and cable connector types. The sensor is connected to the electronics board with a BNC to BNC cable. The electronics board connection to the computer is serial RS232 using a mini-USB to USB cable.

2 Software

The instrument software is written in the C programming language and compiled to run on a Windows PC¹. It does not command or control any of the hardware components. It communicates with the electronics board to read in two voltages. The ratio of these two voltages is scaled to yield the normalized root mean square of the received Sun irradiance, $\sigma(I)/\langle I \rangle$, which is a measure of the received light intensity fluctuation. Each output voltage pair is considered one measurement and they are retrieved by the software at a rate of 1 Hz. The software outputs the corresponding seeing angle and derives the atmospheric coherence length at zenith (r_0).

2.1 Start Up Operation

The instrument software resides on the ACM computer connected to TMFnet IP 192.138.101.129, which runs a Windows 7 (32-bit) operating system. The program has very basic functionality, it runs for 14 consecutive hours (to include daytime) to acquire data at 1 Hz. The output is displayed in a terminal window and the data is saved to a daily file. The program automatically terminates once the 14 hours of data acquisition is completed.

2.2 Task Scheduler Settings

The Windows Task Scheduler is used to automatically re-start the program on a daily basis at a user specified time, the current start time is set to UT 13:00. Manually starting the program is not needed under normal operating conditions. The following are instructions on how to change the daily start time or update the executable file location if it becomes necessary.

2.1.1 Open Task Scheduler

To access the Task Scheduler, click on the lower left corner Windows “Start” icon. Navigate to All Programs → Accessories → System Tools → Task Scheduler (see Figure 2).

¹ The computer automatically assigns a COM port number to the instrument when it is connected to a USB port. The software must match this assigned port number and need to be re-compiled with the correct value (if different).

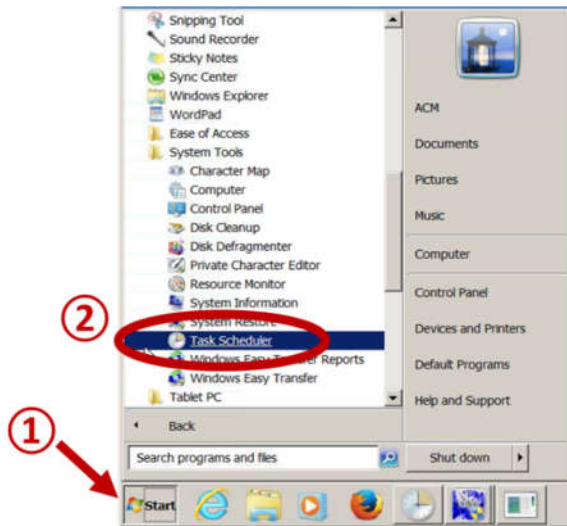


Figure 2: Start menu location to open Task Scheduler.

Start → All Programs → Accessories → System Tools → Task Scheduler

2.1.2 View task properties

In the Task Scheduler window, select “Task Scheduler Library” listed on the left side column. Double-click on the name “Seykora_USB_no4_ro” in the task list as shown in Figure 3. This will open a new window to view and set the various task properties, such as automated start time (section 2.1.3) and program file location (section 2.1.4).

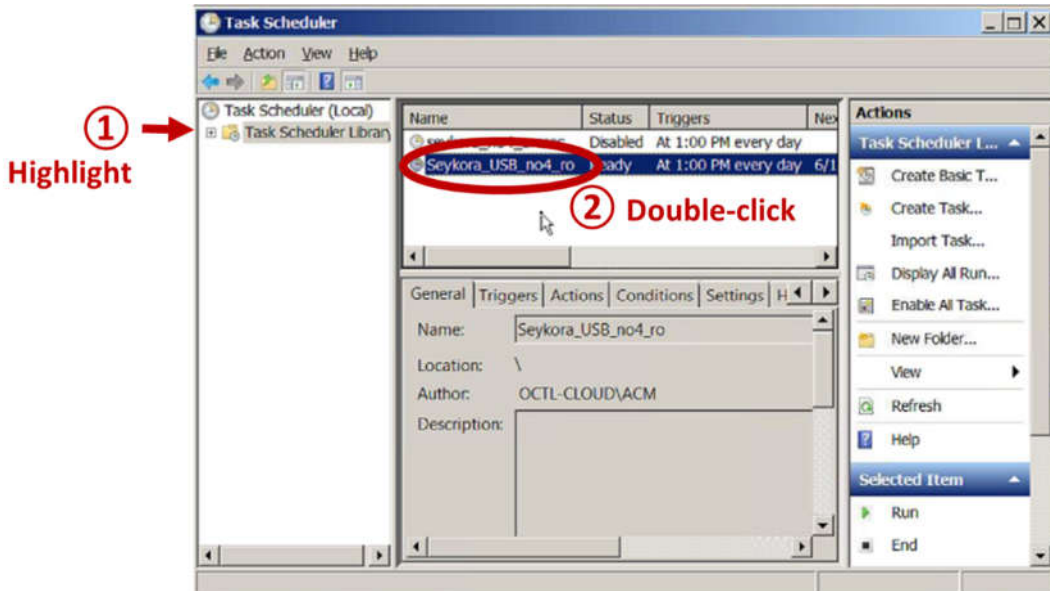


Figure 3: Task Scheduler window steps to view task properties. The settings for automated daily start of the sun scintillometer program is defined in the “Task Scheduler Library” as “Seykora_USB_no4_ro”.

2.1.3 How to update program daily start time

Select “Triggers” among the tabs in the properties window. Highlight the item in the trigger list and click on “Edit”. This will bring up another window where the program start schedule can be updated, click on “OK” if any changes were made. Click on the “OK” button on the properties window to finalize all changes. These steps are also outlined in Figure 4.

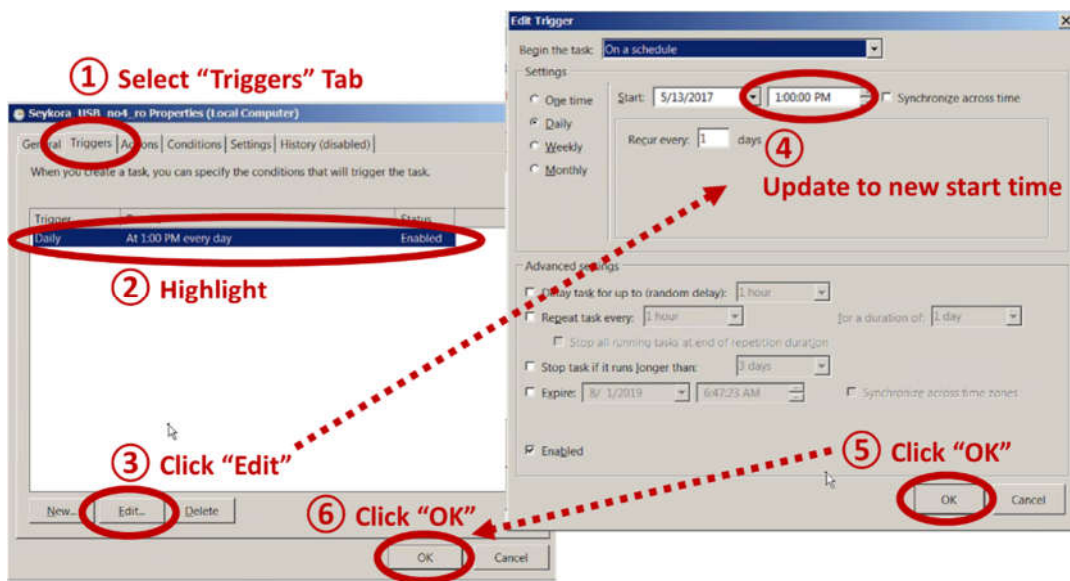


Figure 4: Task Scheduler “Triggers” settings and steps to update automated start time of the program.

2.1.4 How to update program executable file location

Select “Actions” among the tabs in the properties window. Highlight the item in the action list and click on “Edit”. This will bring up another window where the program executable file location can be updated, click on “OK” if any changes were made. Click on the “OK” button on the properties window to finalize all changes. These steps are also outlined in Figure 5.

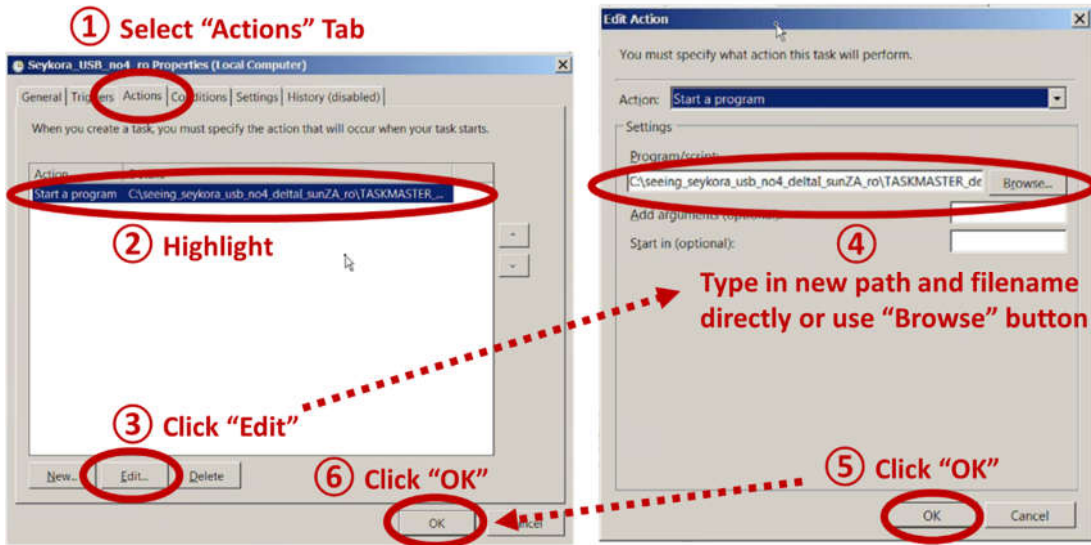


Figure 5: Task Scheduler “Actions” settings and steps to update program executable file location.

2.2 Manual Software Startup and Exit (If Needed)

If there is a need to manually re-start the program, such as recovery from a power outage or computer reboot, the user should make sure to avoid a data acquisition overlap with the next scheduled start of the program by the Task Scheduler. An overlap would mean there are two instances of the program running that will try to read from the electronics board simultaneously and will also write to the same daily data file, either of which may potentially cause unexpected results. If there is a possibility of an overlap, the user should manually terminate the currently running instance before the Task Scheduler starts a new one.

The software source code and data acquisition executable file are located in the following folder.

C:\seeing_seykora_usb_no4_deltal_sunZA_ro

The executable file is named: TASKMASTER_deltal_sunZA_ro.exe

Double-click on the file to start the program and the output terminal window will appear. To manually terminate the program, close and exit the output terminal window.

Alternatively, the program can also be manually started from the Task Scheduler as shown in Figure 6. Right-click on the name of the task and select “Run”. To manually terminate the program instance that was started by the Task Scheduler, right-click on the name of the corresponding task and select “End”.

Select "Run" to start the program.
Select "End" to terminate the program.

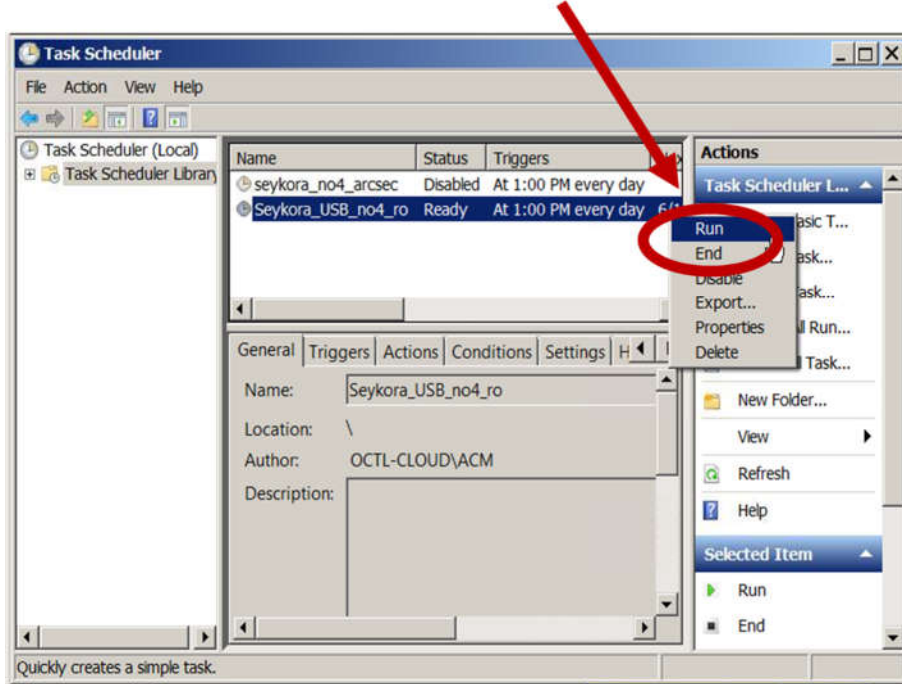


Figure 6: Manual program start or terminate using Task Scheduler.

2.3 Terminal Window Display

Below is a list of output data displayed in the program terminal window as shown in Figure 7. The program also computes a moving average of the received light intensity fluctuation, $(\sigma(I)/\langle I \rangle)$, using the most recent 10 measurements. Data acquisition at a rate of 1 Hz means 10 seconds of data is used in calculating the moving average. This particular value is not output to the display but is saved in the daily data file instead. However, the parameter of most interest (atmospheric coherence length [r_o] at zenith) is derived from the $(\sigma(I)/\langle I \rangle)$ average and the resulting r_o value is included in the display output.

Column 1: Output channel 1 raw intensity;
Column 2: Output channel 2 raw intensity fluctuation;
Column 3: Text field indicating the values are output;
Column 4: Last measured Seykora's seeing angle [as], i.e. $1900 * (\sigma(I)/\langle I \rangle)$, Ref.[1];
Column 5: Solar zenith angle [Deg];
Column 6: r_o [cm] (atmospheric coherence length) at zenith in cm units based on $\sigma(I)/\langle I \rangle$ average ;
Column 7: Astronomical seeing [as] atmospheric coherence length at zenith in arcsec units based on $\sigma(I)/\langle I \rangle$ average ;

0.816	0.610	out1	2.241	32.627	3.310	3.116
0.823	0.606	out1	2.212	32.630	3.321	3.106
0.816	0.597	out1	2.194	32.634	3.341	3.087
0.819	0.606	out1	2.220	32.637	3.368	3.062
0.406	0.619	out1	4.571	32.640	3.379	3.053
0.816	0.603	out1	2.217	32.644	2.982	3.459
0.810	0.594	out1	2.199	32.647	2.908	3.547
0.823	0.590	out1	2.153	32.651	2.901	3.556
0.829	0.568	out1	2.054	32.654	2.905	3.550
0.813	0.558	out1	2.060	32.657	2.924	3.527
0.813	0.552	out1	2.036	32.661	2.947	3.500
0.819	0.532	out1	1.949	32.664	2.977	3.464
0.803	0.103	out1	0.386	32.667	3.017	3.418
0.816	0.513	out1	1.885	32.671	3.319	3.197
0.819	0.487	out1	1.783	32.674	3.382	3.050
0.816	0.477	out1	1.755	32.678	3.995	2.582
0.813	0.490	out1	1.810	32.681	4.116	2.505
0.813	0.706	out1	2.607	32.684	4.224	2.441
0.819	0.313	out1	1.146	32.688	4.099	2.516
0.816	0.526	out1	1.933	32.691	4.357	2.367
0.819	0.529	out1	1.937	32.694	4.396	2.346
0.816	0.523	out1	1.921	32.698	4.426	2.330
0.826	0.519	out1	1.887	32.701	4.435	2.326
0.826	0.529	out1	1.922	32.705	4.010	2.572

Figure 7: Program terminal window display of output data at 1 Hz. Only the first 4 columns of data are shown for the first 10 seconds after initial startup. Columns 5 through 7 : solar zenith angle, r_o [cm] at 500 nm, and astronomical seeing (arcsec). Columns 5 to 7 are displayed after at least 10 measurements are available to calculate a moving average of the light intensity fluctuation $(\sigma(l)/l)$.

3 Data File

The data are saved to a file after each measurement. The program creates a new file each day with filename corresponding to the current UT date and are located in the following folder.

C:\Users\ACM\Documents\seeing_no4_deltal_data

The list of data contained in each file include:

Column 1: UT timestamp with format <year>:<month>:<day>:<hour>:<minute>:<second>;

Column 2: Current $(\sigma(l)/l)$ measurement ;

Column 3: $(\sigma(l)/l)$ moving average of most recent 10 measurements;

Column 4: Current solar zenith angle [deg];

Column 5: r_o [cm] atmospheric coherence length at zenith at 500nm in cm units derived using data in Column 3 and Column 4;

Column 6: Astronomical seeing at zenith at 500nm in arcsec units based on Column 5 value;

Below is an excerpt from one of the data files.

```

2018:07:25:17:00:00 0.001482 0.001335 41.790492 2.912052 3.541661
2018:07:25:17:00:01 0.001443 0.001341 41.787099 2.897195 3.559822
2018:07:25:17:00:02 0.001415 0.001343 41.783705 2.892596 3.565482
2018:07:25:17:00:03 0.001409 0.001338 41.780312 2.905219 3.549990
2018:07:25:17:00:04 0.001409 0.001332 41.776919 2.919974 3.532052
2018:07:25:17:00:05 0.001409 0.001473 41.773526 2.588145 3.984901
2018:07:25:17:00:06 0.001387 0.001467 41.770133 2.601407 3.964586
2018:07:25:17:00:07 0.001428 0.001457 41.766740 2.623050 3.931873
2018:07:25:17:00:09 0.001400 0.001447 41.759954 2.643569 3.901355
2018:07:25:17:00:10 0.001363 0.001431 41.756561 2.679363 3.849235

```

Figure 8: Output data file as measured by the Sun Scintillometer.

4 Theory

Seykora in Ref. [1] introduced first the concept that there is a strong correlation between the scintillation of the solar irradiance measured at ground and the solar image quality. This correlation, in turn, indicates that the astronomical seeing (or the atmospheric coherence length) can be derived by the measurements of the scintillation index of the solar irradiance defined as the normalized of the Sun's Irradiance (I). The scintillation index of the Sun irradiance is defined as

$$(\sigma_I^{sun})^2 = \frac{\langle I^2 \rangle - \langle I \rangle^2}{\langle I \rangle^2} \quad (\text{Eq. 1})$$

To measure the scintillation index of the Sun irradiance, Seykora in [1] introduced a device, composed by a large area APD (Fig. 1), able to provide measurement in real time the value of the normalized std of the sun irradiance, $\sigma(I)/\langle I \rangle = \sigma_I^{sun}$, by measuring the variation of an APD current illuminated by the Sun's Irradiance. According to Ref. [1], $\sigma(I)/\langle I \rangle$ corrected by a proportionality constant was a good measure of the daytime astronomical seeing along the Sun's line-of-sight.

A correction to Seykora's theory was provided by Bekers [2], that related the daytime atmospheric coherence length, r_o , the scintillation index of the irradiance of an extended extraterrestrial source (such as the Sun).

According to Ref. [2], the atmospheric coherence length measured along the ground-to-Sun line-of-sight at zenith angle θ is

$$r_o(\theta, \lambda) = \left[10^{-8} \frac{1.65 h^{-1/3}}{(\sigma_I^{sun}(\theta, \lambda))^2} \cos^{1/3}(\theta) \right]^{3/5} \quad (\text{Eq. 2})$$

Where λ is the wavelength of observation, and $\langle h^{-1/3} \rangle$ is defined as the normalized height of the turbulence, a parameter that is related to the optical turbulence profile and to the coefficient of the structure function of the refractive index, C_n^2 , as

$$\langle h^{-1/3} \rangle = \left(\int_0^{\infty} h^{-1/3} C_n^2(h) dh \right) / \left(\int_0^{\infty} C_n^2(h) dh \right) \quad (\text{Eq. 3})$$

Based on the definition of r_o , one can scale Fried parameter at zenith as

$$r_o(0, \lambda) = \frac{2.1336 \times 10^{-5} \langle h^{-1/3} \rangle^{3/5}}{\sigma_I^{\text{sun}}(\theta, \lambda)^{1.2} \cos^{2/3}(\theta)} \quad (\text{Eq. 4})$$

At the same time, the astronomical seeing at zenith can be expressed as

$$\text{Seeing}(\theta = 0) = \frac{\lambda}{r_o(0, \lambda)} \quad (\text{Eq. 5}).$$

Specifically, the solar scintillometer measurements of the values in Eq. 4 and Eq. 5 are reported in columns 5 and 6 of the output data as in Fig. 8.

5 Previous Measurement Campaign and Validation

Validation of the sun scintillometer's measurements was performed in previous years during different measurement campaigns at JPL. To do this, it was run, side by side, a solar scintillometer and another instrument capable to measure the atmospheric coherence length during daytime, a Solar DIMM [3]. The two instruments measure the atmospheric seeing (and the atmospheric coherence length) observing two different manifestations of the optical turbulence. Particularly, the Solar DIMM derives the atmospheric coherent length by measuring the apparent motion of the limb of the Sun images projected on a camera [3].

Figure 9 illustrates measurements of the atmospheric coherence length performed at Goldstone, CA during four days in July 2007 (time is in UTC). Particularly, in the figure measurements of the atmospheric coherent length at a rate of 10 Hz from the Solar DIMM (blue dots), and by the solar scintillometer (red dots) are reported.

Visual understanding of daily data may be challenging due to: 1) instantaneous variation of the measurement values; and 2) the density of reported values. Figure 10 presents measurement values of the atmospheric coherence length during the day July/31/2007, in this case one can notice that solar scintillometer and Solar DIMM values overlap with good degree of accuracy. However, after filtering the data using a window averaging of 5 minutes, one can visualize how the solar scintillometer and the Solar DIMM measurements are very close, as reported in Fig. 11 where the red solid line (sun scintillometer) and the blue solid line (Solar DIMM) describe the evolution of the atmospheric coherence length during the day. Some differences can be attributed to the fact there the two sensors were separated by a

distance of few meters and therefore they were probing different parts of the atmosphere. Furthermore, both the red line and the blue line follow the diurnal cycle, as expected, with lower values of atmospheric coherence length around noon (strong optical turbulence), and larger values early in the morning when the optical turbulence is expected to be wicker.

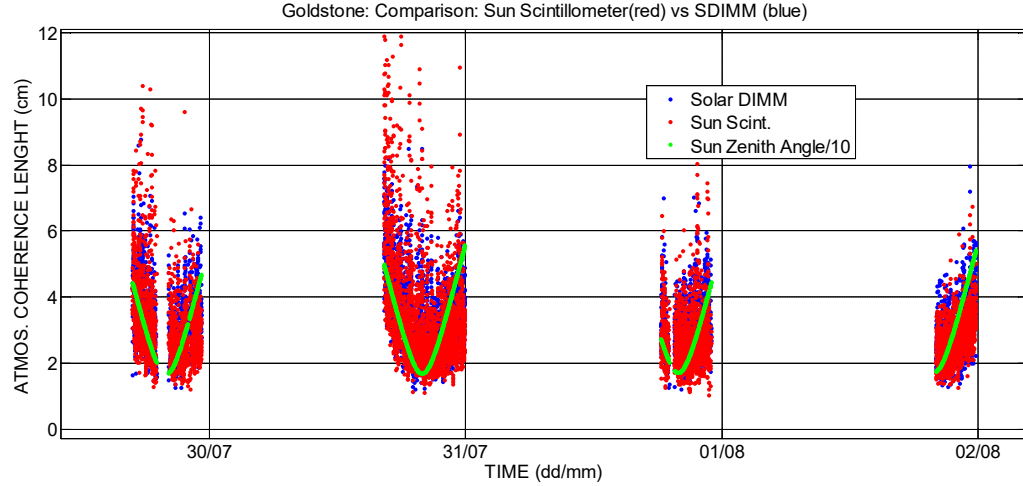


Figure 9: Initial daytime seeing measurement campaign at Goldstone, Summer 2013. Solar scintillometer data (red dots) compared against a Solar DIMM (blue dots). Sun Zenith angle (scaled by a factor of 10) is also reported (green). Notice the lack of data during daytime measurements are due to the presence of clouds.

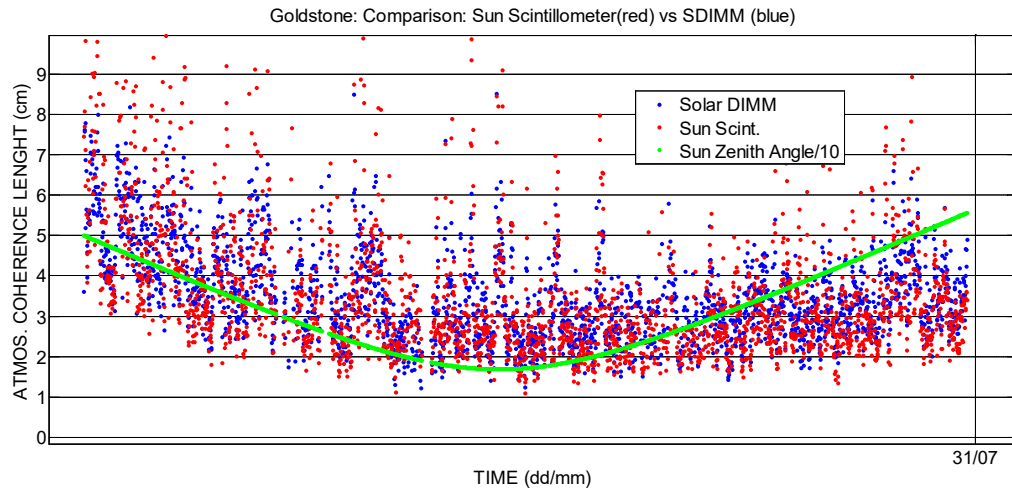


Figure 9: Initial daytime seeing measurement campaign at Goldstone: July/31/2013. Solar scintillometer data (red dots) compared against a Solar DIMM (blue dots). Sun Zenith angle (scaled by a factor of 10) is also reported (green).

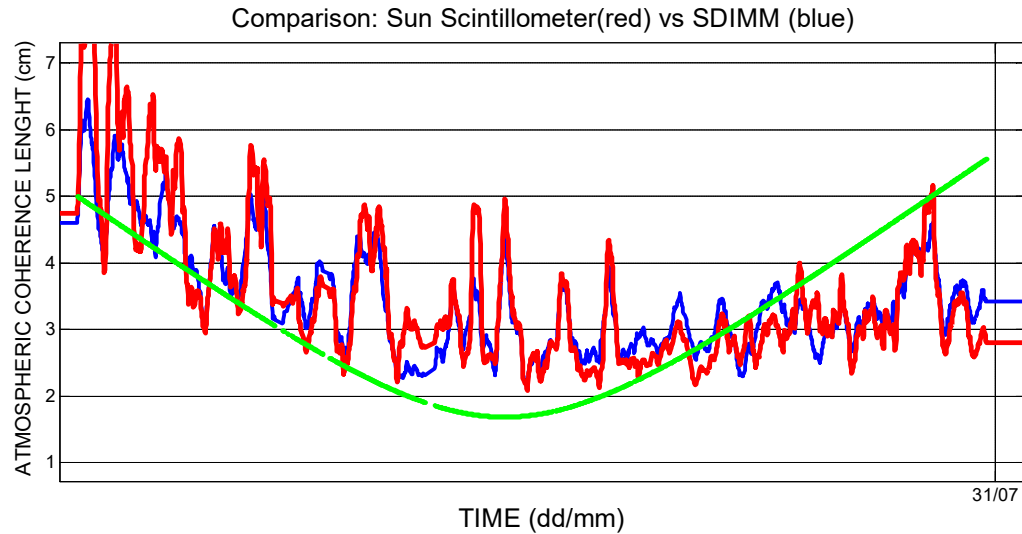


Figure 10: Initial daytime seeing measurement campaign at Goldstone: July/31/2013. Solar scintillometer data (red line) compared against a Solar DIMM (blue line). Sun Zenith angle (scaled by a factor of 10) is also reported (green). Data averaged over 5 minutes.

6 Data Structure

Sun scintillometer data are continuously collected at OCTL for the LCRD program. Particularly, in these report three files are processed:

filter_Seykora_OCTL_no4_ro_20190101_20190114ff.txt;
filter_Seykora_OCTL_no4_ro_20180101_20181231_unique.txt;
filter_Seykora_OCTL_no4_ro_20170501_20171231_unique.txt.

Overall the data cover the period: May 2017 to Jan 2019. Each file consists of six columns:

- 1) MATLAB date-stamp. The update rate is 1 second.
- 2) $\sigma(I)/I$ as measured by the Sun scintillometer along the Sun line-of-sight;
- 3) Average $\sigma(I)/I$ over the last 10 measurements.
- 4) Sun zenith angle;
- 5) Atmospheric Coherence length at 500nm at zenith (using data in 3) and 4));
- 6) Astronomical Seeing at Zenith;

The data are loaded in MATLAB, and then aggregated in a single file, sLCRD.mat

7 Data Description

The data file sLCRD.mat includes a large amount of data, however, post processing/filtering of these data is necessary to provide a robust statistics of the measurement that is ‘noise free’. Rationale for the data filtering/processing is shown in the next sections. It must be noticed, however, that we are mainly interested in considering the data in column 2 of sLCRC.mat file (i.e. $\sigma(I)/I$ values) that are the observables directly measured by the Sun Scintillometer.

Figure 11 shows an example of measurements of $\sigma(I)/I$ for a limited amount of data. The figure is created in MATLAB with the instruction

```
>> plot(sLCRD(2e6:2e6+100000,2),'.').
```

Overall, are shown 1E5 data points with the rate is 1Hz: approximately four days of data are plotted in figure below.

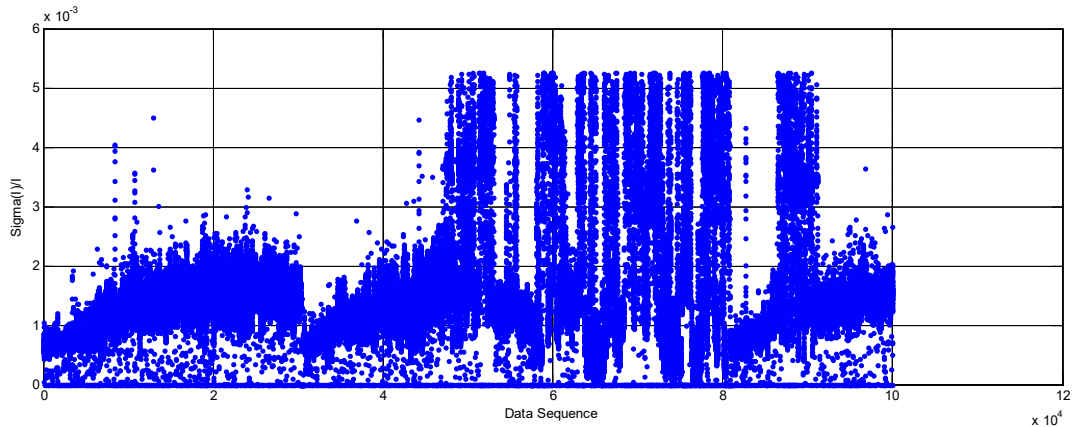


Figure 11. Example of approximately 3 days of $\sigma(I)/I$ measurements by the Sun Scintillometer.

Next, we shortly describe some relevant observations about the data shown in Fig. 11.

Data from one complete cycle of one day is shown in Fig. 12. At the beginning of the day, $\sigma(I)/I$ is usually the lowest and rises in the middle of the day. This is expected. The data at beginning of the day are around 7:00 AM, the data ends around 15:00 PM. The afternoon limit/blockage is due to the Sun obstruction by the OCTL dome. At the moment, we are considering to relocate in order to provide larger observation period (Jan. 14 2019).

The data appear noisy. This can be due to the sensor noise (APD) and to natural variation of the normalized std of the irradiance.

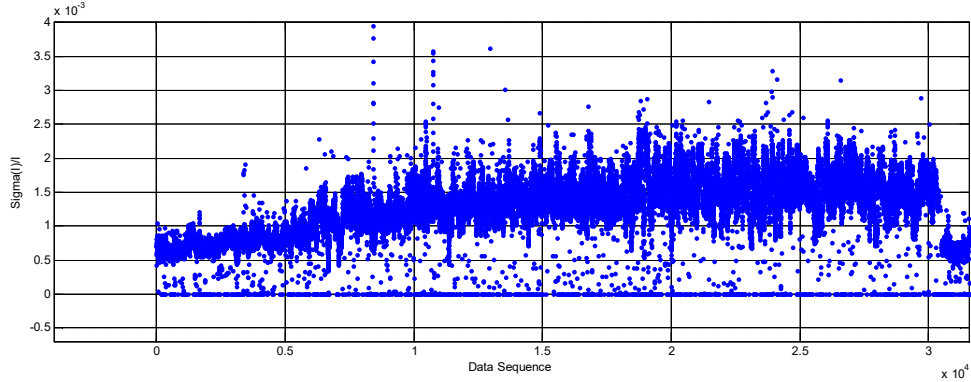


Figure 12. Daily variation of the normalized std of the Sun Irradiance.

There are a number of ‘zero’ values in the measurements. Physically, the zero values should not appear and they can be (easily) removed in the measurements in post-processing. However, it is not clear what is the threshold values for the minimum measured $\sigma(I)/I$: a first analysis suggests to filter out values of $\sigma(I)/I$ between 0 and 0.5E-3. A more detailed analysis on the filtering of low values is in Sec. 7.2. Incidentally, to $\sigma(I)/I=0.5E-3$ corresponds a $r_0=8.4\text{cm}$ at zenith.

The sensor saturates with high values of $\sigma(I)/I$. In this pre-filtered data, the largest (saturation) value is $\sigma(I)/I \sim 5E-3$, Fig. 3. Approximately this value correspond to an $r_0=0.5\text{cm}$ at zenith (at 500nm), which is an extremely low value of atmospheric coherence length. Main cause of this saturation level is due to presence of the clouds, as confirmed by the fact these saturation ‘lines’ are more frequent during winter. Furthermore, it must be pointed out that saturation lines are not isolated, and they have a certain duration. A proper algorithm must be designed to purge saturation lines from the data taking into consideration an interval where the data can be affected by the saturation lines.

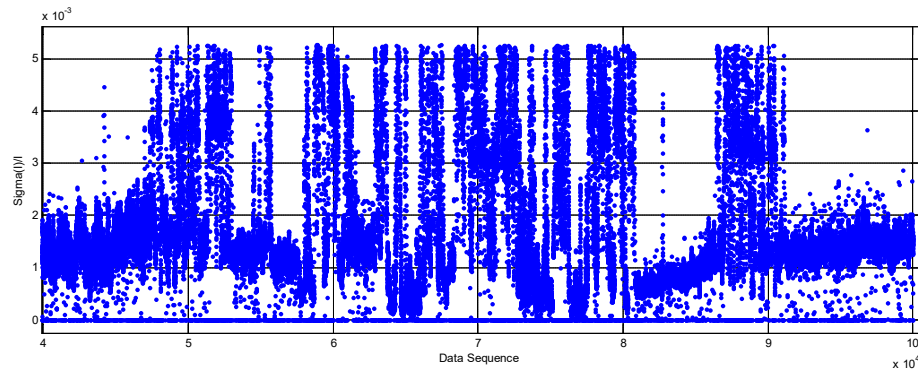


Figure 13. Saturation line due to presence of clouds.

8 Filtering of the data

8.1 Saturation Values

Observing the saturation lines, one can notice that they have a maximum saturation values, and, when saturation occurs, a number of values are also experiencing high values of $\sigma(I)/I$, Fig. 14.

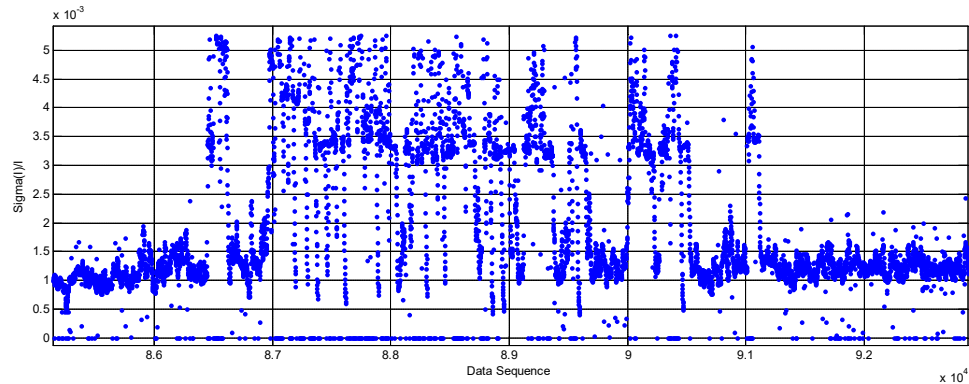


Figure 14. Details of data saturation (due to clouds).

We use the following algorithm to eliminate saturation lines:

- a) Search for values $\sigma(I)/I > 3.5E-3$, and determine the array ‘Indices’ of the index of each value with $\sigma(I)/I > 3.5E-3$. Notice: at $\sigma(I)/I=3.5E-3$, corresponds to $r_0=8\text{mm}$ at zenith at 500nm, we assume that this is a low value of the atmospheric coherence length, and therefore we prefer to filter out these values.
- b) For each index ‘jj’ index in ‘Indices’ set to zero all values in the range ‘jj-30:jj+30’. Notice, the sampling times 10 Hz, in this way, for each saturation value, is eliminated a temporal window of approximately 60 seconds.

Figure 15 presents the same sample data of Fig. 11 with high saturation values filtered out.

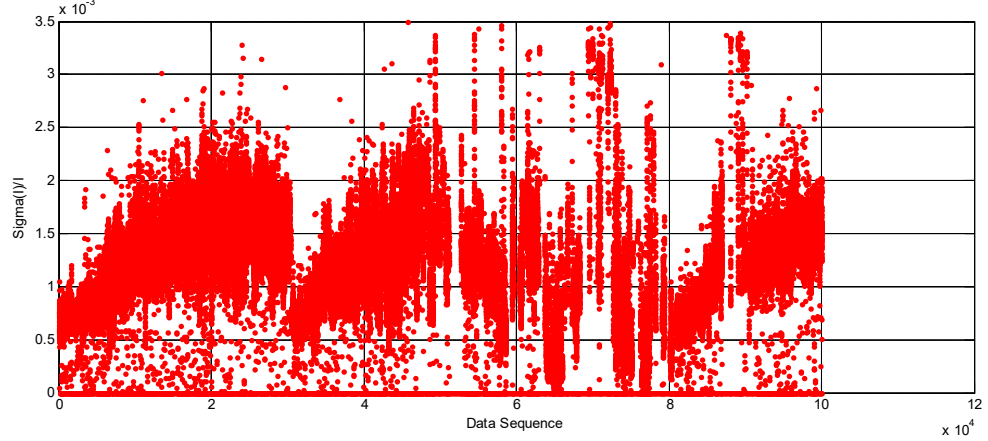


Figure 15. Values of $\sigma(I)/I$ as in Fig. 13: high values of $\sigma(I)/I$ are filtered out set to zero.

8.2 Thesholding Lower Values

After the filtering in Sec. 3.1, there is a large set values with $\sigma(I)/I=0$, physically corresponding to a lack of optical turbulence which is a condition that cannot occur. Consequentially, it is necessary to filter out data below a certain $\sigma(I)/I$ lower threshold that may compromise the overall statistics. Before doing this next filtering of the data, it is necessary to remember that values with $\sigma(I)/I = 0$ are now originated by 1) the initial measurements and 2) by high $\sigma(I)/I$ values filtering as in Sect. 7.1.

Figure 16 plots all values of $\sigma(I)/I$ in sLCRD .mat file in ascending order, after the filtering of the saturation values as in Sec. 7.1. One can notice that the lower knee of the curve is for $\sigma(I)/I$ approximately equal to 0.5E-3, which correspond to $r_0=8.4\text{cm}$ at zenith. It was selected as minimum thereshold $\sigma(I)/I=0.3\text{E-3}$, which correspond to $r_0=15.5\text{ cm}$ at zenith. In other term data with $\sigma(I)/I<0.3\text{E-3}$ were eliminated: overall 3141831 data samples were therefore eliminated, and the new file named **fL4.mat** was created and saved.

File fL4.mat is covering the same period of time of sLCRD.mat, it is composed of 4 columns describing the following fields:

- 1) Column 1, date stamp in MATLAB date format;
- 2) Column 2, normalized std of the Sun irradiance ($\sigma(I)/I$);
- 3) Column 3, atmospheric coherence length (in cm) at zenith at 500 nm. Data derived using Eq. (1) and data in Column 2) and 4);
- 4) Column 4, Sun zenith angle at the time indicated in Column 1.

Figure 17 shows a sub-sample of the measured values after final as in file fL4.mat. One can notice how high saturation values (mainly due to cloud interference) are eliminated, lower values of $\sigma(I)/I$ are also filtered out, daily measurements appear smoother. The data duration here described is approximately

3 days. Figure 18 describes the diurnal variation of the atmospheric coherence length for the same period of time as in Fig. 17 based on $\sigma(I)/I$ measurements of Fig. 17 and Eq. (1).

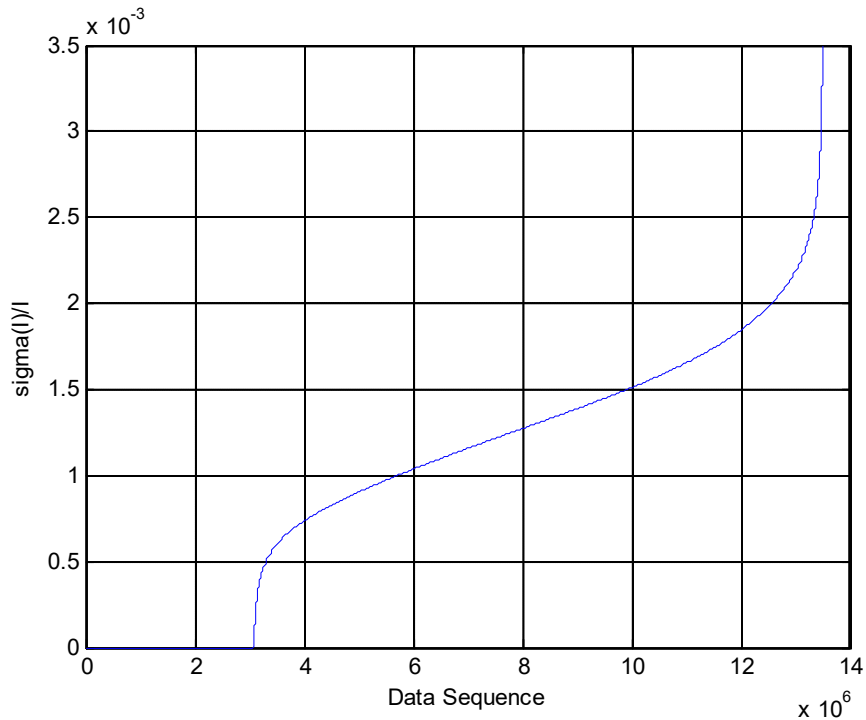


Figure 16. Values of $\sigma(I)/I$ in ascending order of the data set sLCRD.mat after first filtering.

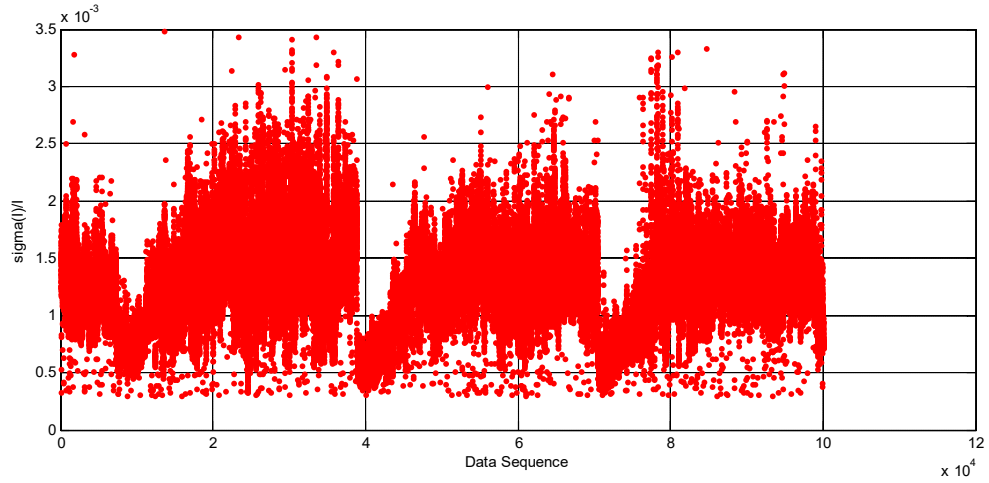


Figure 17. Normalized standard deviation of the solar irradiance after final data filtering for 3 days of data.

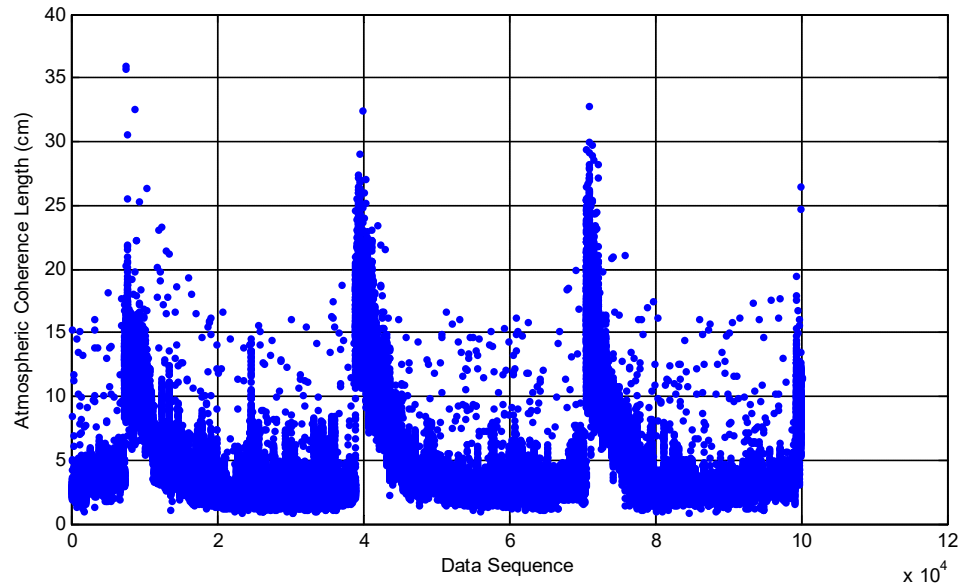


Figure 18. Diurnal variation of the atmospheric coherence length for a sample of filtered data. The data displayed are derived from the $\sigma(I)/I$ values displayed in Fig. 17.

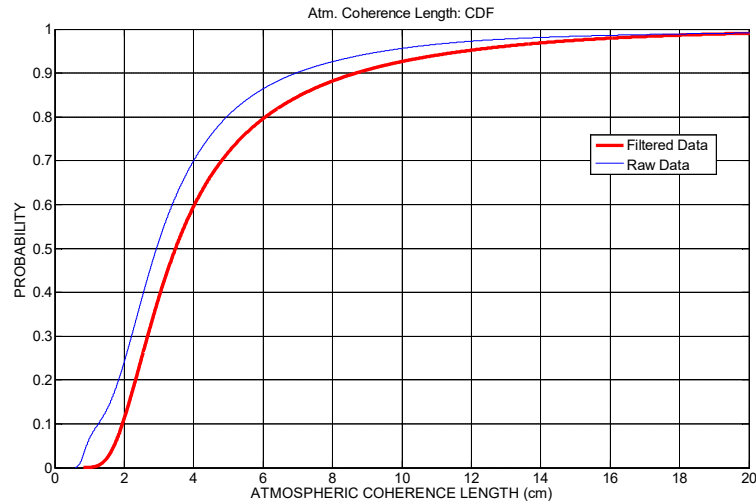


Figure 19. Cumulative distribution function of the atmospheric coherence length of the filtered data (red curve) in fL4.mat file, compared with the overall data in the sLCRD.mat file.

Finally, the filtered data produce a more robust statistics of the atmospheric coherence length. Figure 19 describes the overall cumulative distribution function of the atmospheric coherence length according to the raw data (e.g. file sLCRD.mat) and the filtered data (fL4.mat). According to the filtered

data (red curve), the median of the values corresponds to a $r_0=3.5$ cm, while the 10% of the CDF is approximately 2cm. These values may appear small, however, one must take into consideration that:

- a) daytime values of atmospheric coherence length are smaller than the nighttime values due to the effects of the Sun irradiance and the temperature gradient in air, with emphasis at the ground level;
- b) daytime data collection is limited up to 15:00 PM, due to the fact that the OCTL's dome is obscuring the Sun. This blockage of the Sun does not allow the Sun scintillometer to take more data in the afternoon; at the same time data collected in the later afternoon likely have larger values of atmospheric coherence length and these missing data may limit the overall statistics. In other terms if the measurement were taken from dawn to sunset, one should expect larger values of the atmospheric coherence length than those shown in Fig. 19, for median and 10% values of the.

8.3 Monthly Statistics

Another useful statistic that one can derive from the file fL4.mat is the daytime hourly statistics of the atmospheric coherence length. Figure 20 to Fig. 23 present the average monthly daytime variation atmospheric coherence length as measured by the Sun scintillometer at OCTL.

One may notice that the diurnal variation of the atmospheric coherence length changes on month basis. This is due to the fact the optical turbulence is a function of thermal gradient of the atmosphere profile, which, in turn depends on the solar irradiance and on the sun position (elevation angle). As result of this, we indicated that the strongest turbulence is experienced around noon or early afternoon, when the Sun is high in the sky and the largest Fried parameter is measured around dawn and sunset (not measured here) when there is a thermal equilibrium in the atmosphere from ground to space.

At the same time, because the Sun elevation changes during the year, one can notice that Fried parameter at noon is relatively larger at noon during the winter months (approximately 4cm) respect to noon in the summer months at noon (approximately 2.5cm) when the Sun is highest in the sky and the thermal gradient is the largest.

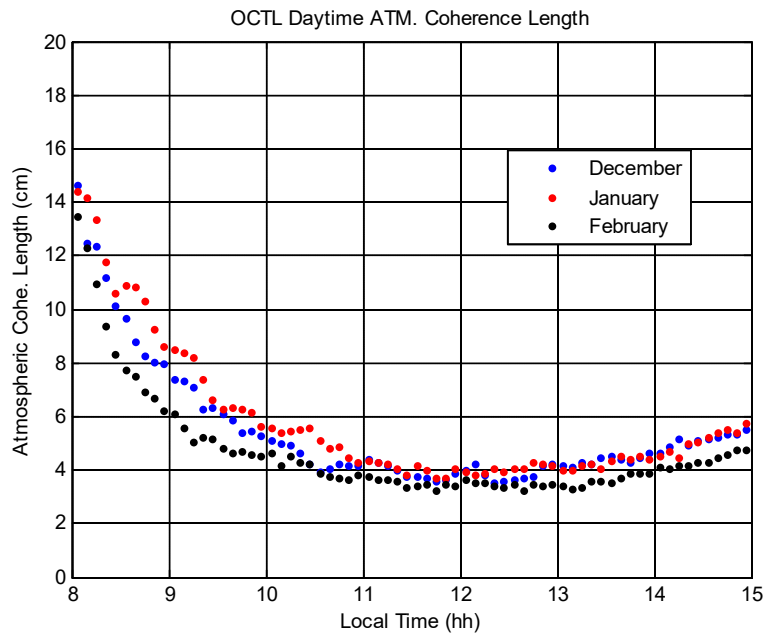


Figure 20. Average diurnal variation at OCTL of the atmospheric coherence length during the winter months.

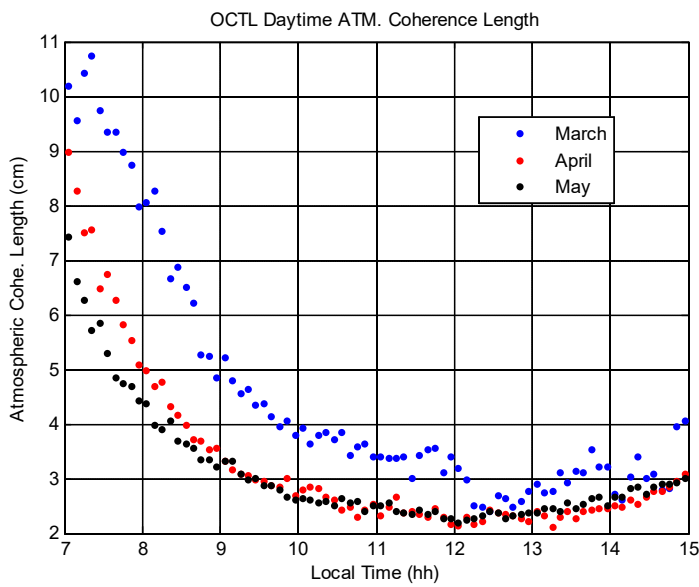


Figure 21. Average diurnal variation at OCTL of the atmospheric coherence length during the spring months.

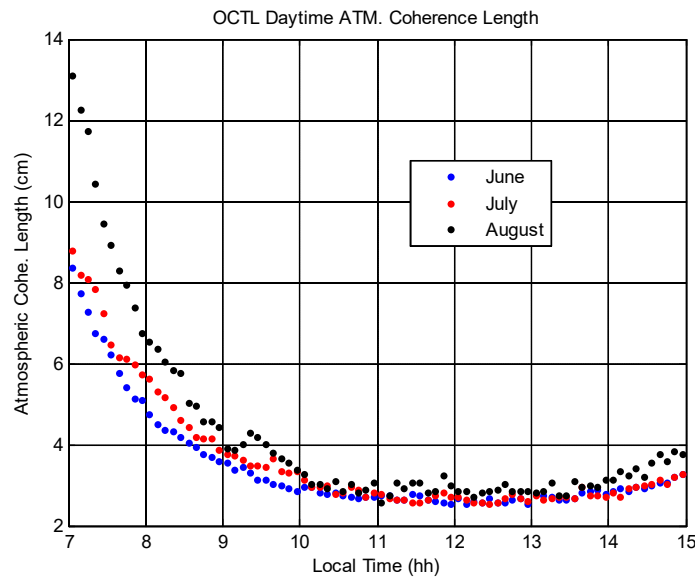


Figure 22. Average diurnal variation at OCTL of the atmospheric coherence length during the spring months.

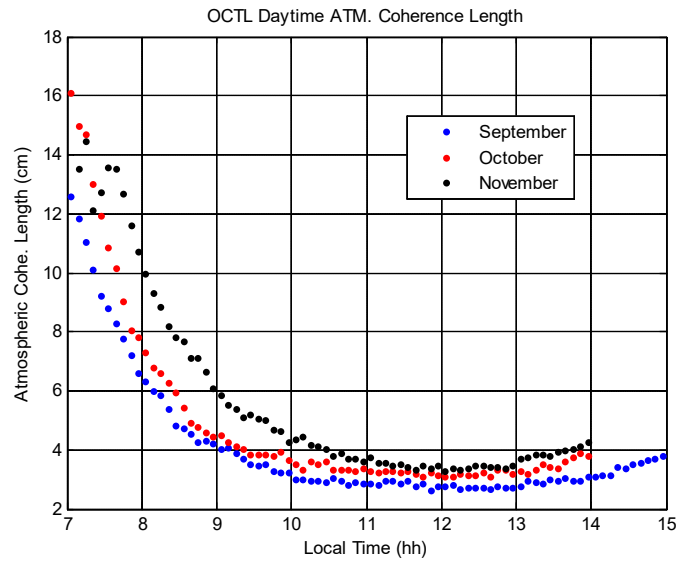


Figure 23. Average diurnal variation at OCTL of the atmospheric coherence length during the fall months.

9 Summary

We have described the deployment of a Sun scintillometer dedicated to provide real time measurements of the daytime atmospheric coherence length.

The first part of this report described the installation of the hardware and of the software of the instrument.

Finally, we have demonstrated how after careful filtering of the data, the measurements of the Sun scintillometer can provide of more robust statistics of the atmospheric coherence length.

10 References

- [1] Seykora, E. J., "Solar Scintillation and the Monitoring of Solar Seeing", *Solar Physics* 145: 389-397 (1993).
- [2] J. M. Beckers, E. Leon, J. Mason and L. Wilkins,' Solar Scintillometry: Calibration of Signals and its Use for Seeing Measurements,' *Solar Physics* 176: 23–36 (1997).
- [3] Jacques M. Beckers,' A Seeing Monitor for Solar and Other Extended Object Observations,' *Experimental Astronomy*, August 2001, Volume 12, Issue 1, pp 1–20